Characterizing transport through a crowded environment with different obstacle sizes

Adam J. Ellery,[1] Matthew J. Simpson,[1,2] Scott W. McCue,[1] and Ruth E. Baker[3]
[1]*School of Mathematical Sciences, Queensland University of Technology, Brisbane, Australia*
[2]*Tissue Repair and Regeneration program, Institute of Health and Biomedical Innovation, Queensland University of Technology, Brisbane, Australia*
[3]*Centre for Mathematical Biology, Mathematical Institute, University of Oxford, Radcliffe Observatory Quarter, Woodstock Road, Oxford, United Kingdom*

(Received 4 November 2013; accepted 20 January 2014; published online 4 February 2014)

Transport through crowded environments is often classified as anomalous, rather than classical, Fickian diffusion. Several studies have sought to describe such transport processes using either a continuous time random walk or fractional order differential equation. For both these models the transport is characterized by a parameter α, where $\alpha = 1$ is associated with Fickian diffusion and $\alpha < 1$ is associated with anomalous subdiffusion. Here, we simulate a single agent migrating through a crowded environment populated by impenetrable, immobile obstacles and estimate α from mean squared displacement data. We also simulate the transport of a population of such agents through a similar crowded environment and match averaged agent density profiles to the solution of a related fractional order differential equation to obtain an alternative estimate of α. We examine the relationship between our estimate of α and the properties of the obstacle field for both a single agent and a population of agents; we show that in both cases, α decreases as the obstacle density increases, and that the rate of decrease is greater for smaller obstacles. Our work suggests that it may be inappropriate to model transport through a crowded environment using widely reported approaches including power laws to describe the mean squared displacement and fractional order differential equations to represent the averaged agent density profiles. © *2014 AIP Publishing LLC*. [http://dx.doi.org/10.1063/1.4864000]

I. INTRODUCTION

Many biological environments, both intracellular and extracellular, are densely crowded by large molecules and cells.[1–3] Therefore, it is important to understand how to characterize and quantify transport processes within such crowded systems. Several previous investigations have sought to describe such process by studying the motion of a single agent moving through an environment that is populated by impenetrable obstacles.[4–13] A standard assumption is that the mean squared displacement (MSD) of a single agent, in two dimensions, averaged over a large ensemble, obeys the power law

$$\langle r^2 \rangle = 4 D t^{\alpha}, \tag{1}$$

where r is the displacement, t is time, and D is a generalized diffusivity.[14–17] The exponent indicates the type of transport, with $\alpha = 1$ for Fickian diffusion and $\alpha < 1$ for anomalous subdiffusion.[14–17] As such, the MSD of a single agent is often thought to be key quantity of interest[18–20] since from it we can estimate α.

As an alternative to studying the motion of a single agent, other experiments have considered the transport of a population of agents.[21] Another standard assumption is that if the MSD of an individual agent obeys Eq. (1), then the transport of a population of such agents obeys a fractional order differential equation (FDE)[14–16,22]

$$\frac{\partial^{\alpha} u}{\partial t^{\alpha}} = D \nabla^2 u, \tag{2}$$

where $u(x, t)$ is the average density of agents and $\partial^{\alpha}/\partial t^{\alpha}$ is a Caputo fractional derivative of order α.[22,23] Equations (1) and (2) are widely used to represent transport through crowded environments.[10–16,22]

In this work, we investigate how obstacle size, shape, and density influences the motion of both a single agent and a population of agents. In Sec. II A, we simulate the motion of a single agent through a crowded environment and estimate α from MSD data. As illustrated by Saxton[4,5] and others,[12] the MSD does not obey Eq. (1) and certain challenges arise when we interpret such data using this power law. We also examine the relationship between our estimates of α and the size, shape, and density of obstacles by repeating our simulations and systematically varying these properties of the obstacles. In Sec. II B, we study the transport of a population of agents and estimate α by matching the solution of Eq. (2) with the observed agent density profiles. Again, we examine how the properties of the obstacle field influence our estimates of α by repeating our simulations and systematically varying the size, shape, and density of obstacles. We also discuss challenges which arise when comparing the solution of Eq. (2) with the population density data. Finally, we summarize our results in Sec. IV, before concluding with some comments about how the present study could be extended. In summary, our work

shows that obstacle size, shape, and density have an important impact on transport through crowded environments, and our data suggest that it may be inappropriate to model transport through a crowded environment using a standard power law description for the MSD or a standard FDE to describe the evolution of the averaged agent density profile.

II. STOCHASTIC SIMULATIONS

We consider a square lattice with lattice spacing Δ, of dimension $M \times N$, where we index sites (i, j), with $0 \le i \le M$ and $0 \le j \le N$, so that each site has location $(x, y) = (i\Delta, j\Delta)$. The lattice dimensions are $0 \le x \le L_x$ and $0 \le y \le L_y$, where $L_x = M\Delta$ and $L_y = N\Delta$. At the beginning of each simulation we randomly populate the lattice with impenetrable immobile obstacles such that the probability that any site is occupied by an obstacle is $\phi \in [0, 0.5]$, which we restrict to be less than the percolation threshold.[24]

In this study, we consider obstacles that occupy: (i) a single lattice site, (ii) two adjacent lattice sites, (iii) four lattice sites in a two by two arrangement, and (iv) nine lattice sites in a three by three arrangement. We refer to these obstacles as 1×1, 1×2, 2×2, and 3×3, respectively. We note that 1×1, 2×2, and 3×3 obstacles are symmetric with respect to the lattice, whereas 1×2 obstacles are asymmetric. In all cases in which we consider 1×2 obstacles, we always ensure that the lattice was populated with, on average, half the 1×2 obstacles aligned along the x axis and half aligned along the y axis.

Our stochastic transport model is an unbiased, nearest neighbour, exclusion process.[25] A Gillespie algorithm[26] is used to advance the simulation until we reach some predetermined inspection time $t = T$. Since we wish to generate averaged data we always consider K identically prepared realizations of each kind of simulation. To reduce computational effort we follow the work of Vilaseca and co-workers[6] and regenerate the obstacle field after every R realizations.

A. Motion of a single agent

After populating the lattice with obstacles, a single agent is placed on a randomly chosen vacant site and allowed to undergo a random walk with periodic boundary conditions applied along all boundaries. For convenience, the MSD data are recorded at geometrically spaced temporal nodes with $t_0 = 0$, $t_{n+1} = t_n + hg^n$, $h = T(1-g)/(1-g^{P-1})$, P is the total number of nodes and $g = 1.1$ is a geometric factor. We rewrite Eq. (1) as

$$\log_{10}\left(\frac{\langle r^2\rangle}{t}\right) = \log_{10} 4D + (\alpha - 1)\log_{10} t, \qquad (3)$$

which implies that if our MSD data follow Eq. (1), plotting $\log_{10}(\langle r^2\rangle/t)$ as a function of $\log_{10} t$ will produce a straight line with slope $\alpha - 1$. Our results in Fig. 1, with the exception of the special uncrowded case, $\phi = 0$, do not give straight lines, which means that the MSD does not obey Eq. (1). This observation is consistent with many previous studies.[4–13] Our data also confirm that as $t \to \infty$, we recover normal diffusion, consistent with prior studies[4–13] (we do not show these long term results here since we are interested in intermediate time scales).

To provide an estimate of α we follow a strategy that has been implemented by others[4–9] and focus on MSD data over intermediate time scales, $10^2 \le t \le 10^3$, since the MSD data are approximately linear during this interval. Using Eq. (3), we estimate α by calculating the slope of the straight line

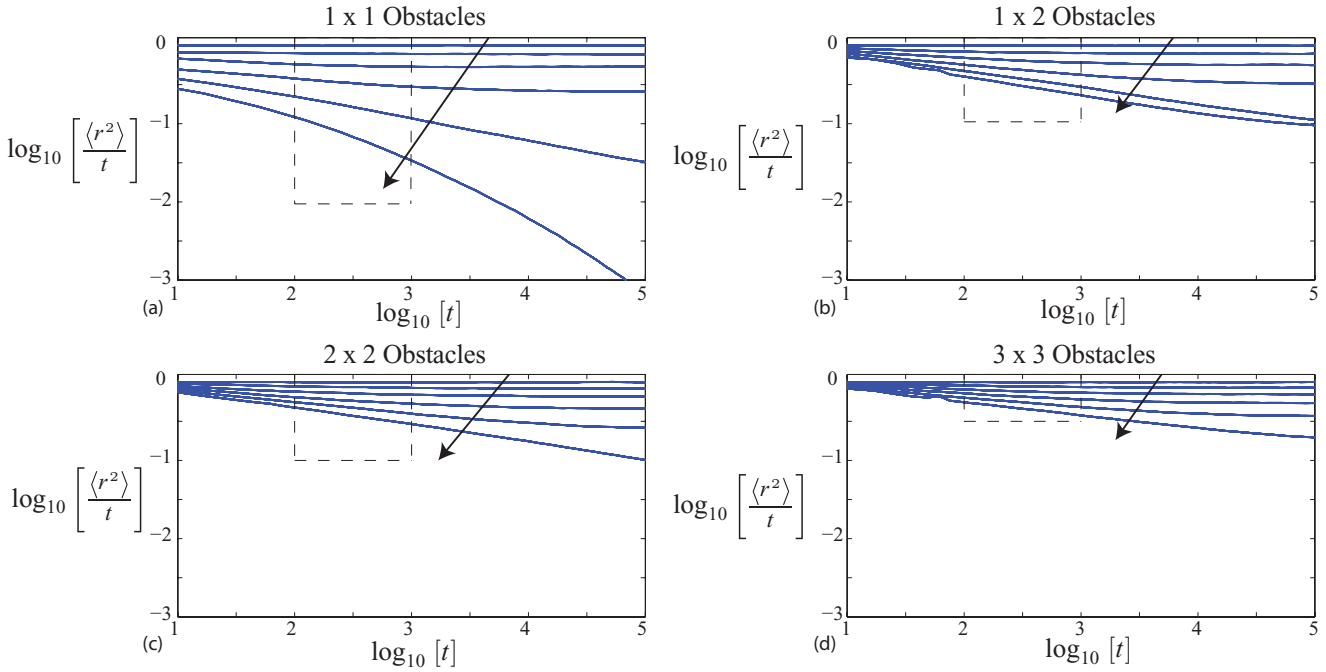

FIG. 1. The MSD (blue-solid) of a single agent. Results in (a), (b), (c), and (d) were generated on a lattice occupied by 1×1, 1×2, 2×2, and 3×3 sized obstacles, respectively. Results are shown for $\phi = 0$, 0.1, 0.2, 0.3, 0.4, and 0.5, with the arrow indicating the direction of increasing ϕ. All results were generated on a 256×256 lattice and were averaged over $K = 50\,000$ realizations. The obstacle field was regenerated every $R = 500$ realizations. The region enclosed by the dashed lines is highlighted in Fig. 2.

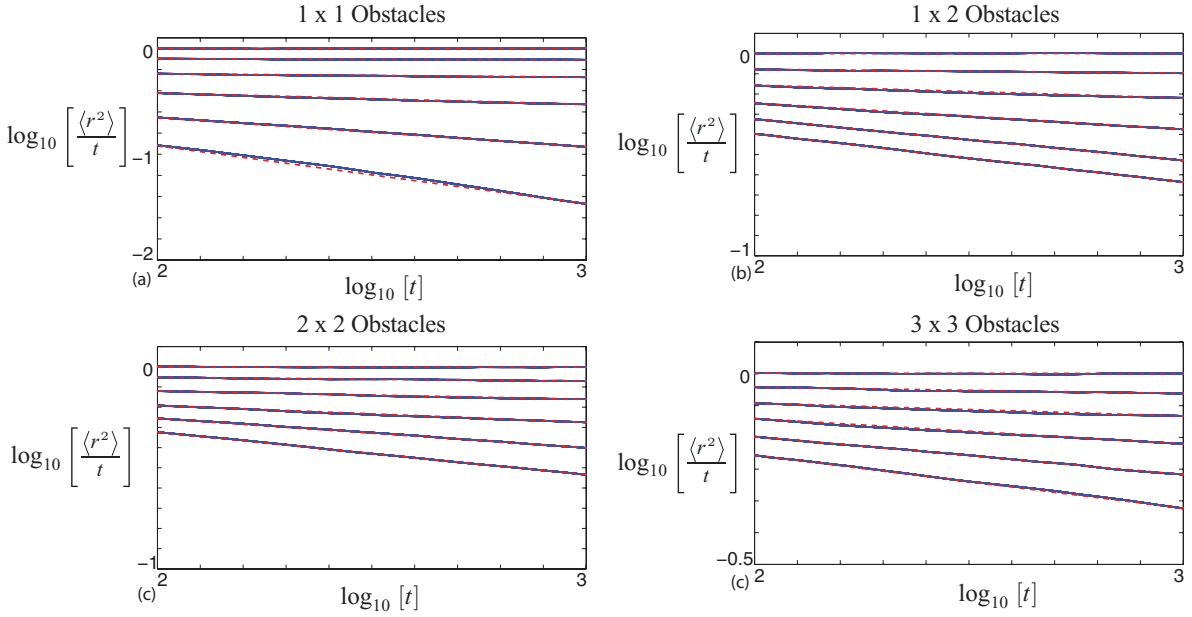

FIG. 2. The MSD (blue-solid) of a single agent. All results are the same as in Fig. 1 except that we focus only on the region $10^2 < t < 10^3$. A straight line (red-dotted) intersecting the ordinate of the MSD data at $t = 10^2$ and $t = 10^3$ is superimposed. Equation (3) indicates that the slope of these lines should be $\alpha - 1$. Corresponding values of α are given in Table I.

intersecting the ordinate of the MSD data at $t = 10^2$ and $t = 10^3$, as highlighted in Fig. 2. To quantify the variability in this estimate of α, we perform the same calculation after shifting the time interval one temporal node to the left, and then one node to the right to provide two additional estimates of α, α_L, and α_R, respectively. We define

$$E_L = \alpha_L - \alpha, \qquad E_R = \alpha - \alpha_R, \tag{4}$$

which allows us to identify an interval, $[\alpha - E_L, \alpha + E_R]$, to indicate the uncertainty in our estimate of α.

Table I summarizes our estimates of α, and the associated uncertainty interval, for all obstacle types. The same data are presented in Fig. 3, with error bars indicating the uncertainty. Our results confirm that when $\phi = 0$ the transport appears to be Fickian diffusion with $\alpha = 1$. Using the strategy just described, for all the obstacle types considered, the transport appears to become increasingly anomalous as ϕ increases, since and our estimate of α decreases with ϕ. Furthermore, the rate at which α decreases with ϕ is different for each obstacle type. For a given value of ϕ, the greatest decrease in α is observed for 1×1 obstacles and the smallest decrease in α is observed for 3×3 obstacles. One way of interpreting this trend is that populating the lattice with larger obstacles leaves larger spaces through which the agents can migrate than occurs for smaller obstacles at the same density. This confirms that obstacle size, shape, and density have an impact on the transport process. We note that the relationship we observe between α and ϕ is qualitatively similar to the results previously reported.[4–6,9]

B. Population of agents

We first randomly populate the lattice with obstacles in the same way that we did in Sec. II A. The simulations are initialized by populating all remaining vacant sites in the vertical strip where $x = 0$ with motile agents. These agents undergo the same random walk procedure described in Sec. II A, except that we have multiple agents on the lattice and potential motility events are aborted if an agent attempts to step to a site that is occupied by either another agent or an obstacle.

TABLE I. The parameter α, estimated using MSD data for 1×1, 1×2, 2×2, and 3×3 obstacles at concentrations $0 \le \phi \le 0.50$ on a 256×256 lattice. Data were averaged over $K = 50\,000$ realizations and the obstacle field was regenerated every $R = 500$ realizations. Estimates of α were calculated using the method described in Sec. II A. The reported variability is the maximum of E_L and E_R, which were calculated using Eq. (4).

ϕ	0.00	0.05	0.10	0.15	0.20	0.25
1×1	$1.00 \pm 8.8 \times 10^{-4}$	$1.00 \pm 1.8 \times 10^{-4}$	$0.99 \pm 1.0 \times 10^{-3}$	$0.98 \pm 2.2 \times 10^{-3}$	$0.97 \pm 1.7 \times 10^{-3}$	$0.95 \pm 1.3 \times 10^{-3}$
1×2	$1.00 \pm 4.5 \times 10^{-4}$	$0.99 \pm 2.1 \times 10^{-3}$	$0.98 \pm 2.1 \times 10^{-3}$	$0.96 \pm 8.3 \times 10^{-4}$	$0.94 \pm 5.0 \times 10^{-3}$	$0.92 \pm 3.9 \times 10^{-3}$
2×2	$1.00 \pm 2.1 \times 10^{-3}$	$0.99 \pm 5.2 \times 10^{-4}$	$0.98 \pm 8.8 \times 10^{-4}$	$0.97 \pm 7.3 \times 10^{-4}$	$0.96 \pm 2.3 \times 10^{-3}$	$0.94 \pm 3.2 \times 10^{-3}$
3×3	$1.00 \pm 2.2 \times 10^{-3}$	$0.99 \pm 3.0 \times 10^{-3}$	$0.98 \pm 2.6 \times 10^{-4}$	$0.97 \pm 7.9 \times 10^{-4}$	$0.96 \pm 6.7 \times 10^{-4}$	$0.94 \pm 3.3 \times 10^{-3}$
ϕ	0.30	0.35	0.40	0.45	0.50	
1×1	$0.90 \pm 4.1 \times 10^{-3}$	$0.81 \pm 3.6 \times 10^{-3}$	$0.72 \pm 4.3 \times 10^{-3}$	$0.56 \pm 8.0 \times 10^{-3}$	$0.44 \pm 1.6 \times 10^{-2}$	
1×2	$0.87 \pm 2.9 \times 10^{-3}$	$0.84 \pm 8.0 \times 10^{-4}$	$0.80 \pm 1.3 \times 10^{-3}$	$0.77 \pm 3.0 \times 10^{-3}$	$0.76 \pm 2.8 \times 10^{-3}$	
2×2	$0.92 \pm 1.5 \times 10^{-3}$	$0.88 \pm 3.0 \times 10^{-3}$	$0.85 \pm 3.3 \times 10^{-3}$	$0.81 \pm 2.1 \times 10^{-3}$	$0.79 \pm 1.7 \times 10^{-3}$	
3×3	$0.92 \pm 4.0 \times 10^{-3}$	$0.90 \pm 9.1 \times 10^{-4}$	$0.88 \pm 6.8 \times 10^{-4}$	$0.86 \pm 3.9 \times 10^{-3}$	$0.83 \pm 2.3 \times 10^{-3}$	

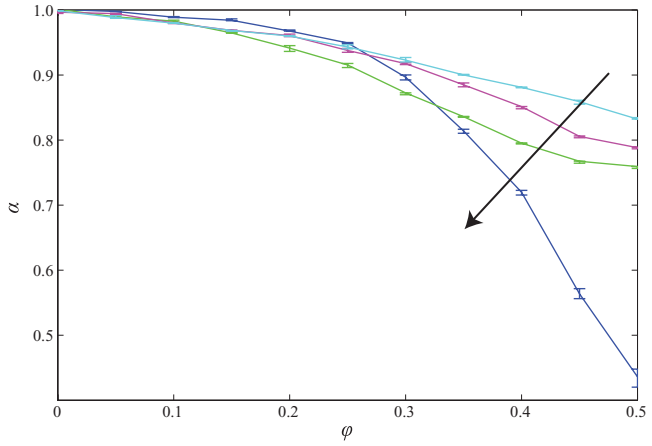

FIG. 3. The dependence of α on the obstacle concentration ϕ, for each obstacle type. Results correspond to 1×1 (dark blue), 1×2 (green), 2×2 (magenta), and 3×3 obstacles (light blue), respectively. The arrow indicates the direction of decreasing obstacle size. Results were generated on a 256×256 lattice and the associated MSD data were averaged over $K = 50\,000$ realizations with $R = 500$. Estimates of α were obtained using the method described in Sec. II A and the error bars indicate the interval, $[\alpha - E_L, \alpha + E_R]$, calculated using Eq. (4).

Periodic boundary conditions are applied along the horizontal boundaries where $y = 0$ and $y = L_y$. As the simulation proceeds, agents that were originally located along the vertical strip with $x = 0$ move from their original location and begin to migrate across the lattice. As soon as one of these agents steps off the vertical strip with $x = 0$ we replace that agent with a new agent ensuring that the density of agents at $x = 0$ remains constant. If, during the simulation, any agent reaches the vertical strip where $x = L_x$, we remove that agent ensuring that the density there remains zero. By considering simulations in which the initial condition is, on average, independent of vertical position, we need only analyze the resulting distribution of agents using one-dimensional density data.[27] For a more general initial condition, we would have to analyze two-dimensional density data.[27]

Once the simulation reaches time T, we construct the average density profiles in the following way: let $n_k(i, j)$ denote the occupancy of site (i, j) during the kth realization such that $n_k(i, j) = 0$ corresponds to a vacant site and $n_k(i, j) = 1$ corresponds to a site occupied by an agent. The average occupancy of sites in the ith vertical strip is

$$\tilde{u}(i\Delta, T) = \frac{1}{K}\sum_{k=1}^{K}\frac{1}{\bar{n}_k}\sum_{j=0}^{N} n_k(i, j), \tag{5}$$

where $\bar{n}_k = \sum_{j=0}^{N} n_k(0, j)$ denotes the number of agents within the vertical strip at $x = 0$ during the kth realization.

To demonstrate how these averaged density profiles correspond to the way that experimental data are presented, we show an image depicting the transport of molecules during the formation of a morphogen gradient in Figs. 4(a) and 4(b),

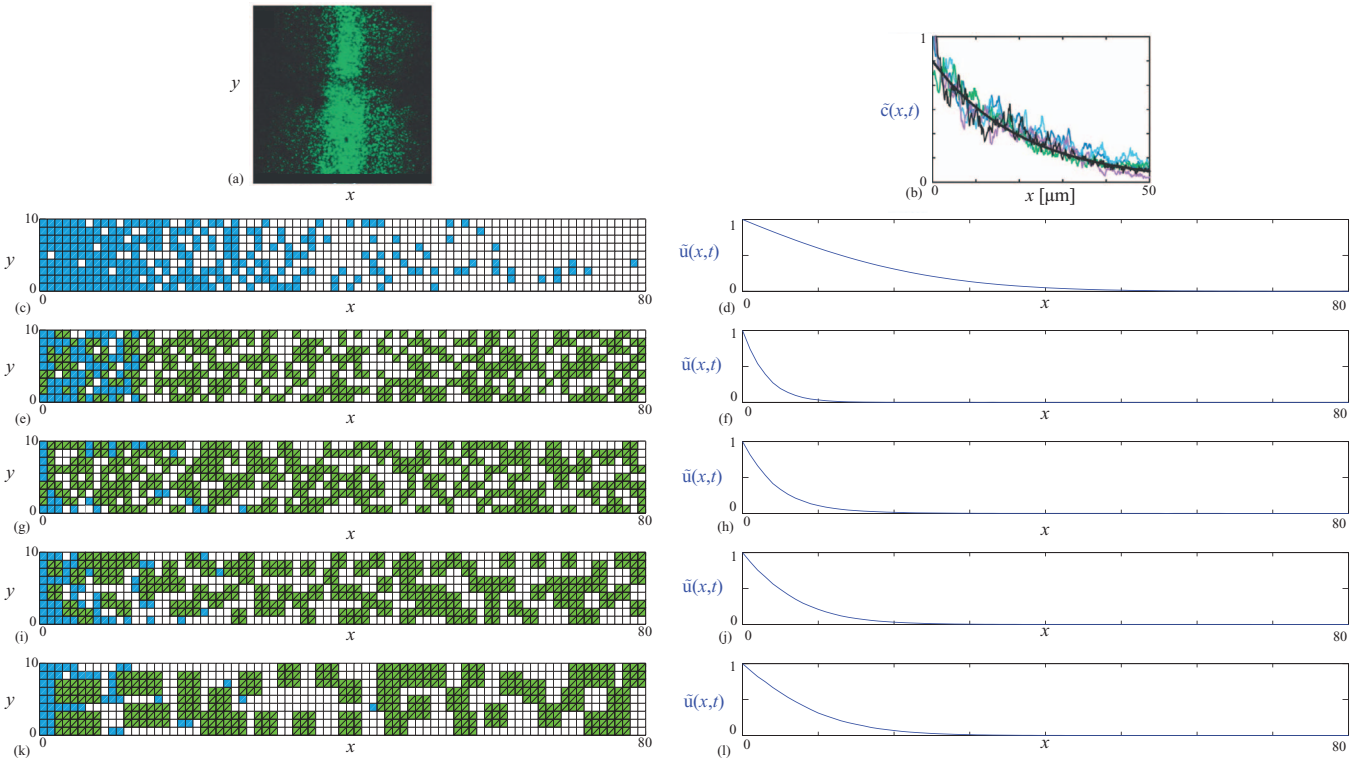

FIG. 4. Images in (a) and (b) show representative experimental results. Reprinted with permission from A. Kicheva, P. Pantazis, T. Bollenbach, Y. Kalaidzidis, T. Bittig, F. Jülicher, and M. González-Gaitán, Science **315**, 521 (2007). Copyright 2007 AAAS.[21] The image in (a) shows the transport of Decapentaplegic (Dpp) in the two-dimensional Cartesian (x, y) plane while the image in (b) shows the corresponding, vertically averaged, one-dimensional density profile advancing in the positive x direction. The remaining images illustrate the results of our discrete model describing the transport of a population of agents (blue) through a lattice populated by impenetrable, immobile obstacles (green, with diagonal). Results in (c)–(d) correspond to a lattice with no obstacles while results in (e)–(f), (g)–(h), (i)–(j), and (k)–(l), correspond to lattices populated by 1×1, 1×2, 2×2, and 3×3 obstacles with $\phi = 0.5$, respectively. Results in (c), (e), (g), (i), and (k) show a single simulation on a 80×10 lattice while results in (d), (f), (h), (j), and (l) show the average agent population density, $\tilde{u}(x, t)$, for an identically prepared suite of simulations on a 100×1000 lattice, with $R = 100$ and $K = 50\,000$. All results are presented at time $T = 1000$.

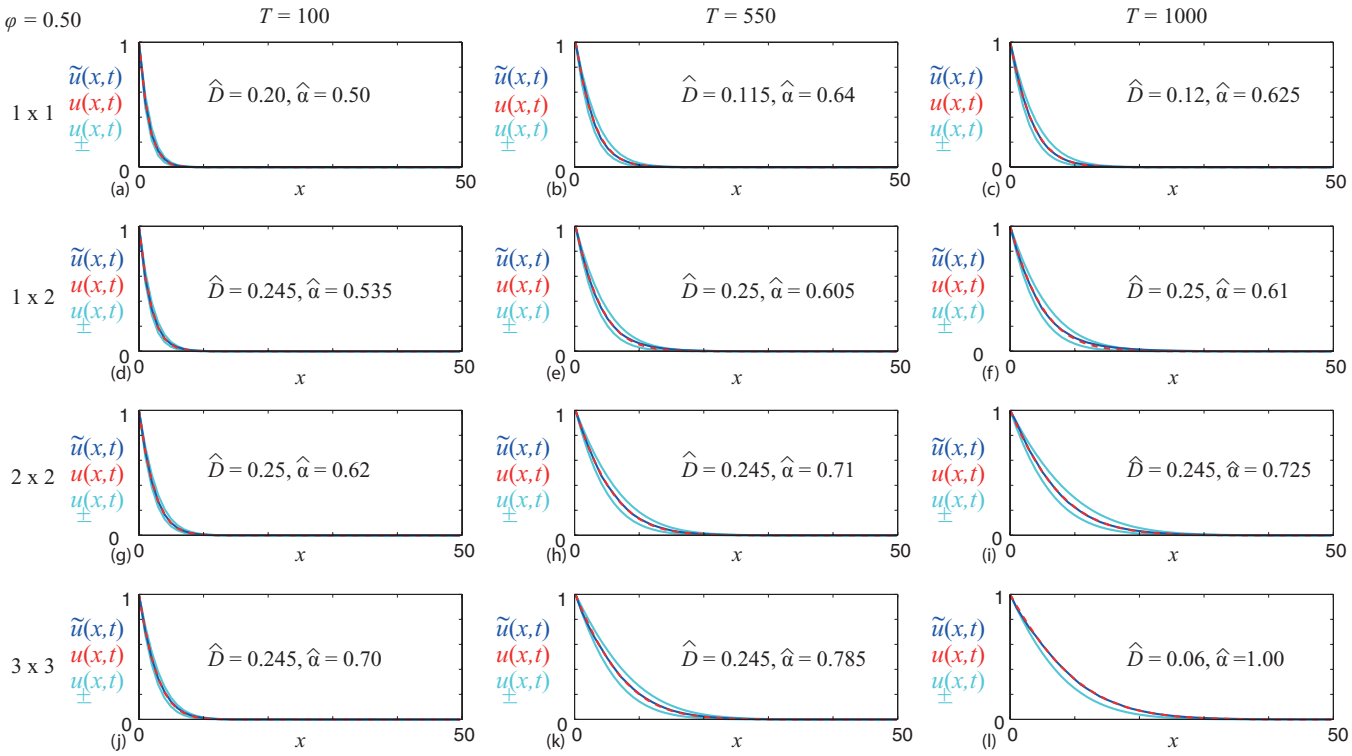

FIG. 5. Averaged agent density data for $\phi = 0.5$. We show the normalized density of agents in each vertical strip, $\tilde{u}(x, t)$ (dark blue), the analytical solution of Eq. (2), $u(x, t)$, with $(\hat{\alpha}, \hat{D})$ (red-dashed) and the analytical solution of Eq. (2), $u_{\pm}(x, t)$, with $\alpha = \hat{\alpha} \pm 0.05$ and $D = \hat{D}$ (light blue), where care was taken to only present results where $\alpha \leq 1$. Results in (a)–(c); (d)–(f); (g)–(i) and (j)–(l) correspond to lattices populated with 1×1, 1×2, 2×2, and 3×3 obstacles, respectively. Results in (a), (d), (g), and (j); (b), (e), (h), and (k); and (c), (f), (i), and (l) correspond to $T = 100$, $T = 550$, and $T = 1000$, respectively. The $\tilde{u}(x, t)$ profiles were generated on a 100×1000 lattice and were averaged over $K = 50\,000$ realizations. The obstacle field was regenerated every $R = 100$ simulations. Results for $u(x, t)$ used parameters $L = 1000$, T as indicated, and the least-squares estimates of $(\hat{\alpha}, \hat{D})$ as given in each subfigure and presented in Table II. The analytical solution was truncated after 50 000 terms in the series.

illustrating both the two-dimensional spatial distribution of molecules as well as the averaged density profiles constructed using a similar vertical averaging procedure.[21] Figures 4(c)–4(l) also show a snapshot of the simulated transport process for each type of obstacle considered together with the corresponding averaged density profile. In Fig. 4(c), we show a snapshot from a single realization of the stochastic model and in Fig. 4(d) we show the averaged agent population density data for $\phi = 0$. Results in Figs. 4(e)–4(l) show a single realization of the stochastic model together with the corresponding averaged agent density data for lattices populated with 1×1, 1×2, 2×2, and 3×3 obstacles, respectively, with $\phi = 0.5$.

The results in Fig. 4 illustrate how the obstacle size, shape, and density affect the transport of a population of agents. In Fig. 4(c), for $\phi = 0$, we observe individual agents almost reach $x = L_x$. In contrast, the profiles in Figs. 4(e), 4(g), 4(i), and 4(k), in which $\phi = 0.5$, show that agents in a crowded environment are unable to move as far. If we compare snapshots in Figs. 4(e), 4(g), 4(i), and 4(k), we observe that the distance the agents move in the positive x direction varies with the size and shape of the obstacles even though ϕ is the same. These results imply that 1×1 obstacles are more effective at retarding the collective motion than 3×3 obstacles at the same ϕ. The trends in the individual snapshots from the stochastic model are consistent with the averaged density data in Fig. 4(d), 4(f), 4(h), 4(j), and 4(l).

To explore how the averaged density profiles change with time, we present $\tilde{u}(x, T)$ in Fig. 5. These results show that the distance the density profile propagates in the positive x direction increases with time; however, we observe different behaviour depending on the shape and size of the obstacles. In particular, the 1×1 obstacles have a greater impact on the average density profile than 3×3 obstacles at the same ϕ. Note that all results in Fig. 5 are for $\phi = 0.5$ and additional results for $\phi = 0$ and $\phi = 0.25$, which illustrate the same trends, are given in Figs. 7 and 8 of the supplementary material.[28]

III. FRACTIONAL ORDER DIFFERENTIAL EQUATION MODEL

We now attempt to use a standard approach to model the transport process described in Sec. II B using Eq. (2). Since the MSD of a single agent does not follow Eq. (1), it seems reasonable to suppose that Eq. (2) may not be an appropriate representation of this transport process. Despite this possible weakness, we are interested in determining how well Eq. (2) describes this transport process, since modeling transport through crowded environments using a FDE framework is a standard approach.[14–17,31–33] To achieve this goal, we determine estimates of α and D such that the solution of the one-dimensional version of Eq. (2) matches our observed density data, and we examine how these estimates vary with obstacle size, shape, density and simulation time.

The appropriate boundary and initial conditions are $u(0, t) = 1$, $u(L_x, t) = 0$, and $u(x, 0) = 0$, where we have normalized the density at $x = 0$ to be unity. For these conditions, the solution of the one-dimensional version of Eq. (2) is[22]

$$u(x,t) = \frac{L_x - x}{L_x} - \sum_{n=1}^{\infty} \left(\frac{2}{n\pi}\right) \sin\left(\frac{n\pi x}{L_x}\right) \mathrm{E}_\alpha \left[-D\left(\frac{n\pi}{L_x}\right)^2 t^\alpha\right], \tag{6}$$

where $\mathrm{E}_\alpha[z]$ is the Mittag-Leffler function.[22]

To estimate α and D we match Eq. (6) to our averaged agent density data using the Levenberg-Marquardt (LM)[29,30] nonlinear least-squares parameter estimation algorithm. We first define a measure by which Eq. (6) can be compared to our averaged density data

$$\epsilon_i = u(i\Delta, T) - \tilde{u}(i\Delta, T), \tag{7}$$

where $u(i\Delta, T)$ is given by Eq. (6) and $\tilde{u}(i\Delta, T)$ is the averaged agent density data. The LM algorithm minimizes $\mathcal{S}(\alpha, D) = \sum_{i=0}^{M} \epsilon_i^2$, by taking an initial estimate, (α_0, D_0), and moving along the surface $\mathcal{S}(\alpha, D)$ to find the least-squares value, $(\hat{\alpha}, \hat{D})$, where $\mathcal{S}(\hat{\alpha}, \hat{D})$ is a minimum. To implement the LM algorithm, we restrict our search to that region of the parameter space where $0.5 \leq \alpha \leq 1$ and $0 < D \leq 0.25$.

The error surfaces, $\mathcal{S}(\alpha, D)$, for each obstacle type and density are given in Figs. 9–12 of the supplementary material.[28] On each error surface we indicate $(\hat{\alpha}, \hat{D})$ and found that the LM algorithm converged to the same $(\hat{\alpha}, \hat{D})$, regardless of (α_0, D_0). Our estimates of $(\hat{\alpha}, \hat{D})$ are summarized in Table II. For $\phi = 0$, the error surface is relatively shallow at $T = 100$, whereas by $T = 550$ the error surface has a more clearly defined minimum with $(\hat{\alpha}, \hat{D}) \approx (1, 0.25)$, as we expect.[27] For simulations with $\phi > 0$, the error surfaces are relatively shallow for all T considered meaning that there is a large region of the parameter space in which $\mathcal{S}(\alpha, D)$ is almost constant. For a given simulation time, T, and obstacle density, $\phi > 0$, there are a number of $(\hat{\alpha}, \hat{D})$ pairs for which $u(x, t)$ matches the observed data equally well. Our estimates of $\hat{\alpha}$ and $\hat{D}$ appear to vary with the simulation time, and $\hat{\alpha}$ tends to increase with T. In summary, these results imply that associating a $(\hat{\alpha}, \hat{D})$ pair with our simulation data is problematic since it is unclear which combination of parameters we should use at a given time, or at what simulation time, T, we should measure them.

To examine the sensitivity of the solution of Eq. (2), $u(x, t)$, to variations in our estimate of $\hat{\alpha}$ we plot $u(x, t)$, with $\hat{\alpha} \pm 0.05$ and $\hat{D}$, in Fig. 5. In generating these sensitivity results we only report results where $\alpha \leq 1$. For cases in which $\hat{\alpha} + 0.05 > 1$ we do not plot an additional solution. Comparing the solutions with $\hat{\alpha} \pm 0.05$ to the original solution with $\hat{\alpha}$ in each subfigure of Fig. 5 indicates that the results at $T = 100$ are relatively insensitive to our choice of α. In contrast, the solution at $T = 1000$ shows that we have an increased sensitivity to the value of α.

IV. DISCUSSION

In this work, we presented a discrete model of transport through a crowded environment that is randomly populated with impenetrable, immobile obstacles. We focused on developing an understanding of how obstacle shape, size, and density affect the transport process by collecting two different kinds of data. We first considered the motion of a single agent by reporting on the MSD data, which does not obey Eq. (1). To make progress using this power law, we estimated α by assuming that the data could be approximated by Eq. (1) within a representative time interval. We fitted a straight line to the data within this time interval for each obstacle density and shape considered.

Our estimates of α from the MSD data indicate that the degree to which the transport can be interpreted as anomalous depends on the obstacle size, shape, and density. As the obstacle density, ϕ, increases, our estimate of α decreases. Regardless of the extent to which our MSD data can be described using Eq. (1), our simulations confirm that obstacle size, shape, and density have a major impact on the transport process.

We then separately considered the transport of a population of agents through a crowded environment using the same random walk framework, except that we considered

TABLE II. The anomalous diffusion parameter, $\hat{\alpha}$, and the diffusion coefficient, $\hat{D}$, for averaged agent population data. Parameters were approximated by matching stochastic data generated using the algorithm described in Sec. II B to Eq. (6) using the Levenberg-Marquardt algorithm.

		1 × 1 obstacles		1 × 2 obstacles		2 × 2 obstacles		3 × 3 obstacles	
	Time	$\hat{D}$	$\hat{\alpha}$	$\hat{D}$	$\hat{\alpha}$	$\hat{D}$	$\hat{\alpha}$	$\hat{D}$	$\hat{\alpha}$
	100	0.17	1.00	0.17	1.00	0.17	1.00	0.17	1.00
$\phi = 0.00$	550	0.21	1.00	0.21	1.00	0.21	1.00	0.21	1.00
	1000	0.22	1.00	0.22	1.00	0.22	1.00	0.22	1.00
	100	0.25	0.745	0.25	0.77	0.25	0.81	0.12	1.00
$\phi = 0.25$	550	0.09	1.00	0.1	1.00	0.125	1.00	0.145	1.00
	1000	0.09	1.00	0.105	1.00	0.13	1.00	0.150	1.00
	100	0.20	0.50	0.245	0.535	0.25	0.62	0.245	0.70
$\phi = 0.50$	550	0.115	0.64	0.25	0.6050	0.245	0.71	0.245	0.785
	1000	0.12	0.665	0.25	0.61	0.245	0.725	0.06	1.00

simulations containing many agents. In these simulations the motion of a particular agent is affected by the presence both the obstacles and other agents. For these simulations we chose initial conditions and boundary conditions so that we could describe this transport process using one-dimensional, vertically averaged, density profiles.[27] To provide information about how the obstacle size, shape, and density affect this averaged agent density profile, we performed many realizations and systematically varied properties of the obstacle field. Our suite of density profiles again shows that smaller obstacles are more effective at retarding the motion of the density profile than larger agents placed at the same density.

In an attempt to describe the transport of a population of agents through a crowded environment using a continuum mathematical model,[14–16,31–33] we applied a FDE to our averaged density data. To estimate how well the FDE model matched the data, we calibrated α and D so that the solution of the FDE matched our averaged density data. This procedure confirmed that the transport process depends on the obstacle size, shape, and density with our estimate of α decreasing with ϕ. We also found that smaller obstacles led to a greater decrease in α than larger obstacles placed randomly at the same density and that, generally, our estimate of α increases with the simulation time.

In summary, our work has raised two key issues with respect to modelling transport through crowded environments. First, we have shown that obstacle size, shape, and density play a key role. This is an important point to highlight since many previous studies have dealt exclusively with one type of obstacle only.[4,5] Furthermore, those studies which have considered obstacles of different size examined MSD data without any explicit consideration of averaged density information.[4–7,9] One of the limitations of our work is that we only considered one type of obstacle whereas it might be more realistic to consider simulations where the lattice is populated by multiple types of obstacles of different shapes and sizes in the same simulation.

A second key issue relates to the difficulties we experienced when attempting to parameterize a standard FDE description of the averaged density profiles. Despite the widespread use and analysis of FDE models,[14–16,31–33] our attempt to fit the solution of Eq. (2) to our density data produced least-squares estimates of α that are strongly dependent on the inspection time. This implies that Eq. (2) does not describe the averaged properties of our discrete model, since any use of Eq. (2) implicitly assumes that α is constant. Indeed, these observations are consistent with the fact that the MSD data of a single agent for the equivalent process do not follow the widely reported power law, given by Eq. (1). We conclude that FDE models should be used with great care when modelling transport through crowded environments since our work shows that data from a relatively simple random walk process cannot be described using a FDE.

ACKNOWLEDGMENTS

We appreciate the comments from two anonymous referees and support from the Australian Research Council (FT130100148).

[1] M. Weiss, M. Elsner, F. Kartberg, and T. Nilsson, Biophys. J. **87**, 3518 (2004).
[2] R. J. Ellis, Trends Biochem. Sci. **26**, 597–604 (2001).
[3] J. A. Dix and A. Verkman, Annu. Rev. Biophys. **37**, 247 (2008).
[4] M. J. Saxton, Biophys. J. **66**, 394 (1994).
[5] M. J. Saxton, Biophys. J. **72**, 1744 (1997).
[6] E. Vilaseca, A. Isvoran, S. Madurga, I. Pastor, J. Garcés, and F. Mas, Phys. Chem. Chem. Phys. **13**, 7396 (2011).
[7] E. Vilaseca, I. Pastor, A. Isvoran, S. Madurga, J. Garcés, and F. Mas, Theor. Chem. Acc. **128**, 795 (2011).
[8] A. Isvoran, E. Vilaseca, F. Ortega, M. Cascante, and F. Mas, J. Serb. Chem. Soc. **71**, 75 (2006).
[9] A. Isvoran, E. Vilaseca, L. Unipan, J. Garcés, and F. Mas, Rev. Roum. Chim. **53**, 415 (2008).
[10] A. Wedemeier, H. Merlitz, C.-X. Wu, and J. Langowski, J. Chem. Phys. **127**, 045102 (2007).
[11] A. Wedemeier, T. Zhang, H. Merlitz, C.-X. Wu, and J. Langowski, J. Chem. Phys. **128**, 155101 (2008).
[12] A. Wedemeier, H. Merlitz, C.-X. Wu, and J. Langowski, J. Chem. Phys. **131**, 064905 (2009).
[13] A. Wedemeier, H. Merlitz, and J. Langowski, Europhys. Lett. **88**, 38004 (2009).
[14] R. Metzler and J. Kladter, Phys. Rep. **339**, 1 (2000).
[15] I. M. Sokolov, J. Klafter, and A. Blumen, Phys. Today **55**, 48 (2002).
[16] B. Henry, T. Langlands, and S. Wearne, Phys. Rev. E **74**, 031116 (2006).
[17] J.-P. Bouchaud and A. Georges, Phys. Rep. **195**, 127 (1990).
[18] D. S. Banks and C. Fradin, Biophys. J. **89**, 2960 (2005).
[19] G. Guigas, C. Kalla, and M. Weiss, Biophys. J. **93**, 316 (2007).
[20] H. Sanabria, Y. Kubota, and M. N. Waxham, Biophys. J. **92**, 313 (2007).
[21] A. Kicheva, P. Pantazis, T. Bollenbach, Y. Kalaidzidis, T. Bittig, F. Jülicher, and M. González-Gaitán, Science **315**, 521 (2007).
[22] I. Podlubny, *Fractional Differential Equations* (Elsevier Science, 1998).
[23] K. Oldham and J. Spanier, *The Fractional Calculus* (Dover Publications Incorporated, 2006).
[24] D. Stauffer and A. Aharony, *Introduction to Percolation Theory* (Taylor and Francis, 1992).
[25] T. M. Liggett, *Interacting Particle Systems* (Springer, 2005).
[26] D. T. Gillespie, J. Phys. Chem. **81**, 2340 (1977).
[27] M. J. Simpson, K. A. Landman, and B. D. Hughes, Physica A **388**, 399 (2009).
[28] See supplementary material at http://dx.doi.org/10.1063/1.4864000 for plots of $\tilde{u}(x,t)$ with $\phi = 0.00, 0.25$ (Figs. 7 and 8) and images of the error surfaces (Figs. 9– 12).
[29] D. W. Marquardt, J. Soc. Ind. Appl. Math. **11**, 431 (1963).
[30] K. Levenberg, Q. Appl. Math. **2**, 164 (1994).
[31] S. B. Yuste, L. Acedo, and K. Lindenberg, Phys. Rev. E **69**, 036126, (2004).
[32] S. B. Yuste and K. Lindenberg, Phys. Rev. Lett. **87**, 118301 (2001).
[33] E. Abad, S. B. Yuste, and K. Lindenberg, Phys. Rev. E **81**, 031115 (2010).